Solar radiation characteristics at the INO BSRN station

E. CARSTEA[1,*], K. FRAGKOS[2]
[1]*National Institute of Research and Development for Optoelectronics - INOE 2000, 077125, str. Atomiştilor nr. 409, Măgurele, Romania*
[2]*Department of Resilient Society, Eratosthenes Centre of Excellence, Limassol, Cyprus*

Solar radiation significantly influences Earth's climate and ecosystems. Accurate solar radiation data, including intensity and frequency, are vital for solar power utilization and understanding climate patterns. South East Europe, and Romania specifically, holds substantial solar energy potential. The study focuses on analysing a dataset of two-year, high-quality solar radiation components at a station near Bucharest, part of the Baseline Surface Radiation Network. Analysis of 2021-2022 solar radiation reveals key solar fluctuations, emphasizing significant peaks in July. The data underline the region's unique solar radiation profile, valuable for future renewable energy planning.

(Received October 23, 2024; accepted December 2, 2024)

Keywords: Solar radiation, BSRN station, Clearness index

1. Introduction

Solar radiation is a fundamental component of Earth's energy balance, playing a vital role in driving the planet's climate, ecosystems, and energy production. Accurate measurements of solar radiation are essential for understanding Earth's climate system and developing renewable energy systems, particularly solar energy [1]. In recent years, significant progress has been made in the photovoltaics technology of harnessing solar energy, by developing new material design and synthesis [2-4], improving architecture [5, 6] and optimizing output [7, 8]. However, in order to use solar energy as a power source, information regarding radiation intensity and frequency distribution is needed [9]. In addition, it is important to determine the seasonal variation of the quantity of solar radiation and the number of days with values below or above the limits of global solar radiation and its components, beam, diffuse and ground reflected radiation [9, 10].

Large regions of South East Europe have been shown to have high solar energy potential [11]. Particularly, in Romania, several regions have been identified as highly suitable for solar energy systems [12]. So far, the solar energy potential has been determined, in Romania, using global solar radiation measurements, provided by the National Meteorological Agency in the period 1983- 2005, and satellite data SIS-SARAH [13]. The SIS-SARAH dataset offers high temporal resolution (15-minute intervals) and high spatial resolution (0.05° × 0.05°), spanning from 1983 to the present [14]. These data are particularly valuable as they not only provide detailed and reliable information on solar radiation but also enable the monitoring of changes in climatic conditions over time, making them crucial for long-term solar energy planning and adaptation strategies.

This study aims to provide comprehensive information regarding the components of solar radiation (global, diffuse and direct normal short-wave irradiance, and longwave downward irradiance), measured at a Baseline Surface Radiation Network (BSRN) station (hereafter named INO station) in South West of Bucharest, Romania. The BSRN is coordinated by the World Meteorological Organization (WMO) [15], and is formed of high-quality, ground-based stations, with state-of-the-art electronic devices, that monitor and record surface radiation. Its primary mission is to provide reliable, accurate and long-term observations of surface radiative fluxes, which are crucial for understanding Earth's radiation budget, climate variability and climate change [16]. The INO Station (Magurele, Romania), situated at Magurele Centre for Atmosphere and Radiation Studies (MARS), was established in December 2019. MARS station is equipped with novel optoelectronic instruments for active and passive remote sensing of the atmosphere, in situ analysis of aerosols and particles, and meteorological stations [17, 18]. As of 2021, the fully operational INO radiation station officially became a member of BSRN network, after a successful evaluation of its quality assurance and quality control (QA/QC) procedures, and it consistently contributes with data to the network's research efforts.

In this study, we conducted a statistical analysis covering the first two years of station operation (2021-2022). These measurements can provide crucial information about the region's specific solar radiation characteristics, which can be used to refine climate models, validate satellite-based and modelled estimates of surface radiation, and optimize solar energy systems. Furthermore, these first-of-their-kind ground measurements in South East Europe can assist researchers to better understand the region's unique solar radiation

dynamics, which will be invaluable for planning future renewable energy projects.

2. Experimental

The INO station (N44.34, E26.01, 111 m elevation) is equipped with various instruments for measuring solar and atmospheric downward radiation components. It includes a Kipp&Zonen SOLYS2 sun-tracker, two Kipp&Zonen CMP22 pyranometers for measuring global and diffuse short-wave irradiance, one Kipp&Zonen CHP1 pyrheliometer for direct normal short-wave irradiance and one shaded Kipp&Zonen CGR4 pyrgeometer for longwave downward irradiance measurements. The pyranometers, the pyrheliometer and the pyrgeometer use passive thermal sensing elements named thermopiles. These sensing elements are covered by a non-spectrally selective, black surface coating, which absorbs energy and heats up the thermopile. The generated heat flows through a thermal resistance in the detector housing, creating a temperature difference. This temperature difference is converted into voltage, linear to the absorbed solar irradiance.

In order to improve the reliability and accuracy of the measurements by reducing thermal offsets, the two pyranometers and the pyrgeometer are equipped with Kipp&Zonen CVF4 Ventilation Units. The instruments collect data at a rate of one-second and are recorded by a Campbell Scientific CR1000X data-logger. From this high-frequency data, one-minute averages, standard deviations, as well as maximum and minimum values are calculated. Finally, both the one-second and one-minute data are stored at MARS data centre.

A two-dimensional representation of the different shortwave and longwave solar radiation components is shown in Fig. 1. The sunrise and sunset hours (magenta dashed lines) were calculated using the solar position algorithm, developed by the National Renewable Energy Laboratory (NREL) [19] and integrated in the pvlib Python package [20]. Periods with missing and removed bad quality data (e.g., during the cleaning of the dome) are displayed as white stripes. Considering the geographic location of INO station, the sun's transit time was expected at around 10:15 UTC, varying from 10:00 to 10:30 due to the Earth's axial tilt. However, it is quite hard to determine the exact transit time from Fig. 1, especially during the autumn-winter months, since clouds often cover Magurele area [21].

For the QA/QC, the BSRN recommended tests [22, 23] were applied for data collected between 2021-2022. To compute the monthly mean values two years of data (excluding the missing days) were used. The data were averaged from 1-minute measurements to 15-minute intervals. These were then averaged into 1-hour intervals and finally into daily mean values. The statistical analysis was applied to the daily means.

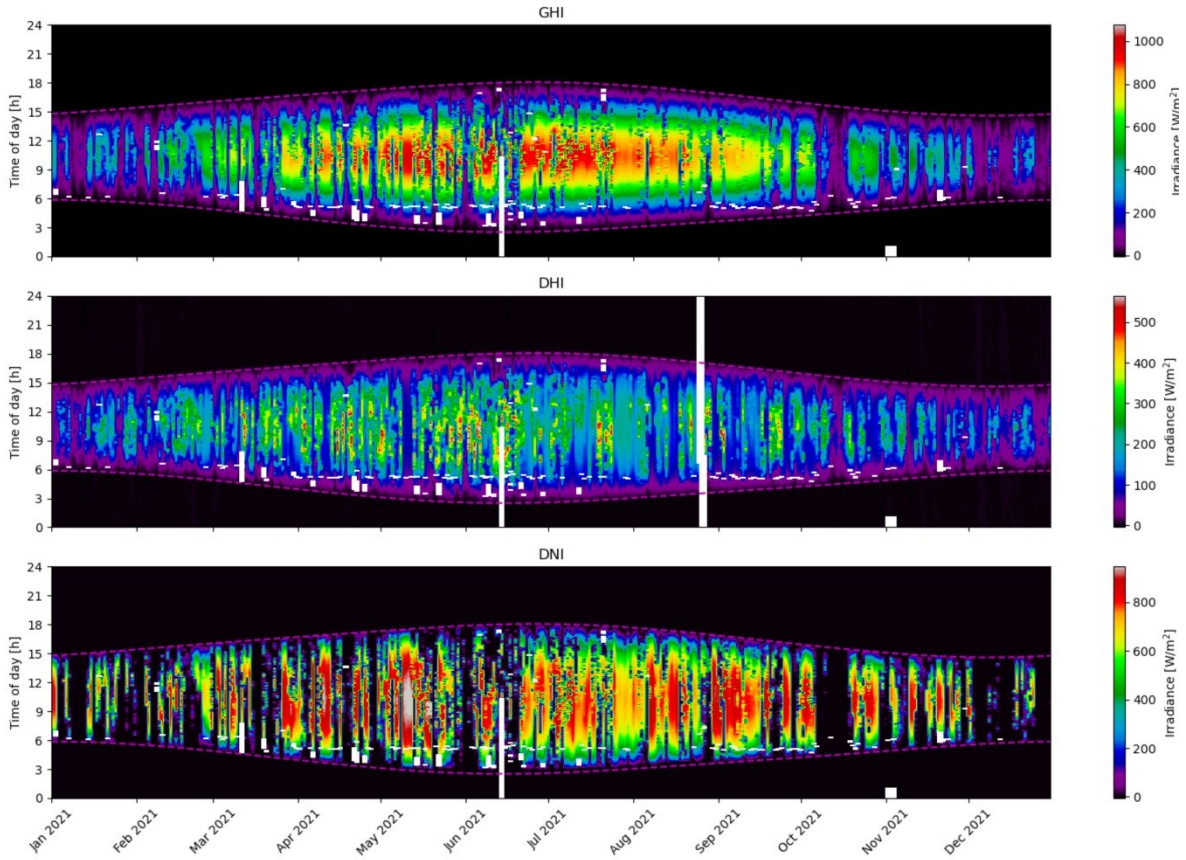

(a)

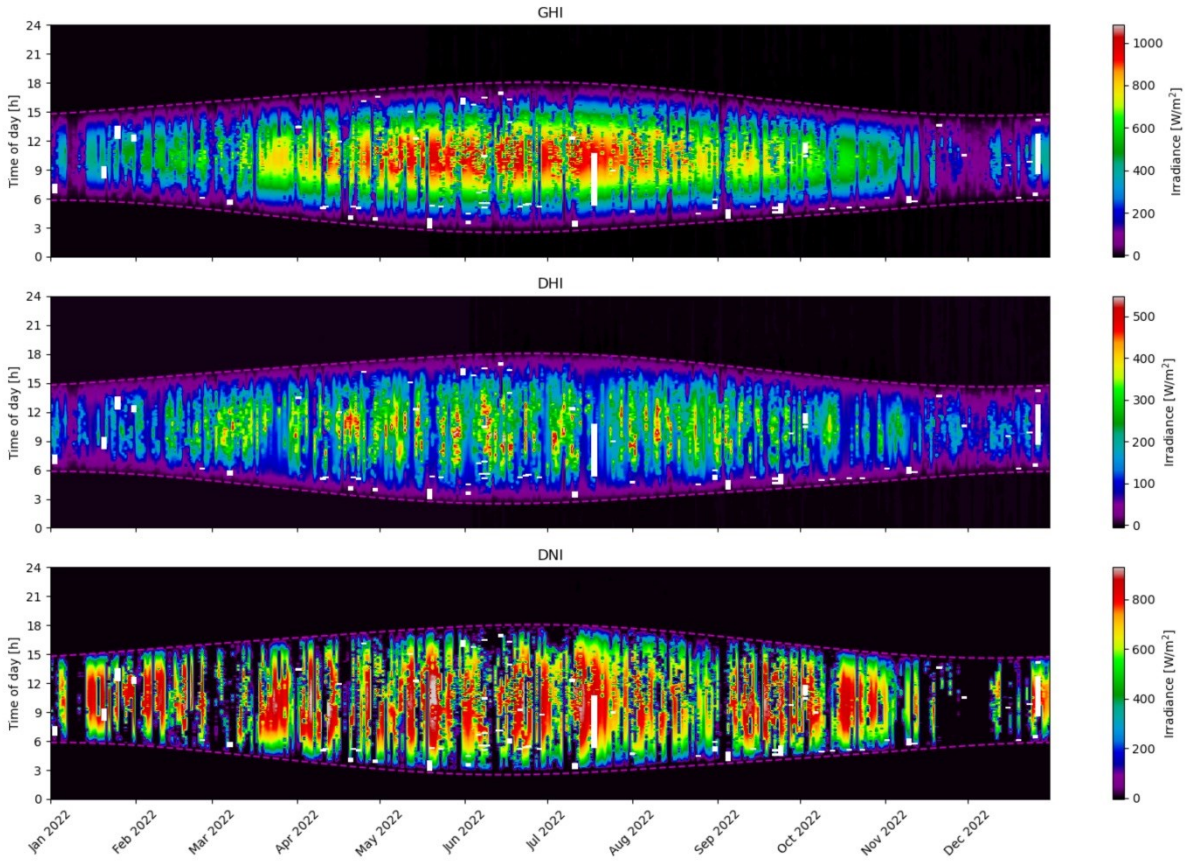

(b)

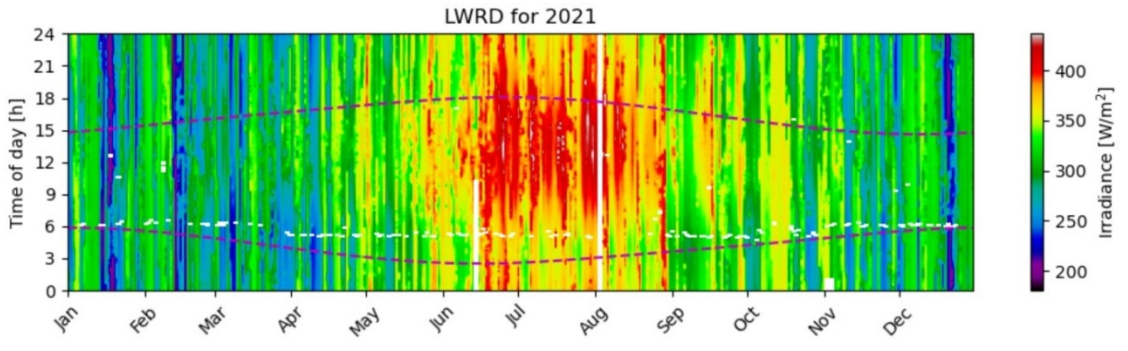

(c)

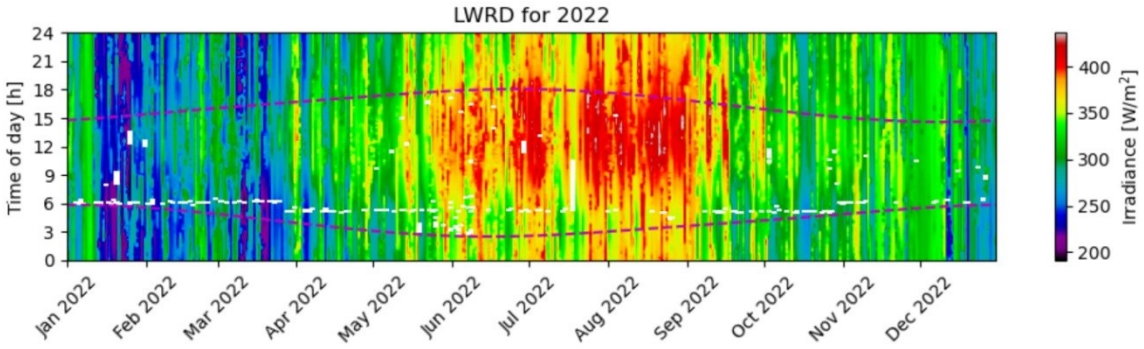

(d)

Fig. 1. Two dimensional representations of global horizontal (GHI), diffuse (DHI) and direct normal (DNI) irradiance measurements (a & b) and longwave downward irradiance (LWRD) (c & d) for 2021-2022. Missing values are indicated by white areas during daytime, between sunrise and sunset times (represented in magenta dash lines). The x-axis corresponds to days and the y-axis to the hour of the day in UTC. Please note that there is a different irradiance scale for each panel (color online)

3. Results and discussions

3.1. Statistics of monthly mean GHI values

The monthly mean values of the global horizontal irradiance (GHI) and its components, diffuse horizontal irradiance (DHI) and direct normal irradiance (DNI), for the years 2021 and 2022, are shown in Fig. 2. An evident annual pattern is discernible, characterized by lower values during the winter months and higher values during the summer. Additionally, distinct characteristics related to various meteorological conditions, primarily associated with cloud coverage, can be observed. In 2021, the monthly mean GHI ranged from 87 W/m^2 in December to 459 W/m^2 in July, resulting in a difference factor of 5.29. While for 2022, the monthly mean values of GHI varied from 110 W/m^2 in December to 468 W/m^2 in July, representing a difference factor of 4.25. Lower values were recorded in June compared to May, in both years, due to increased cloudiness recorded in June relative to the other summer months. In June, the highest mean DHI values were also recorded. In the first six months, the monthly mean GHI values were slightly higher in 2022 compared with 2021, driven by the higher DNI values recorded for 2022. The statistics of monthly mean GHI values are shown in Table 1. The median values are higher than mean values in most months, with the highest median values on July 2021 and July 2022. The coefficient of variation (CV) shows the stability of the parameter over a time interval [9]. The CV is relatively high in both years, varying between 12 % and 67 % in 2021, and between 14 % and 61 % in 2022, considerably higher compared to the values reported by Kalogirou et al. [9] for the Mediterranean area. The lowest CVs, for both years, were found for July and August, indicating a relatively stable atmosphere. The highest CVs were obtained in the winter, when higher daily changes in weather conditions are seen.

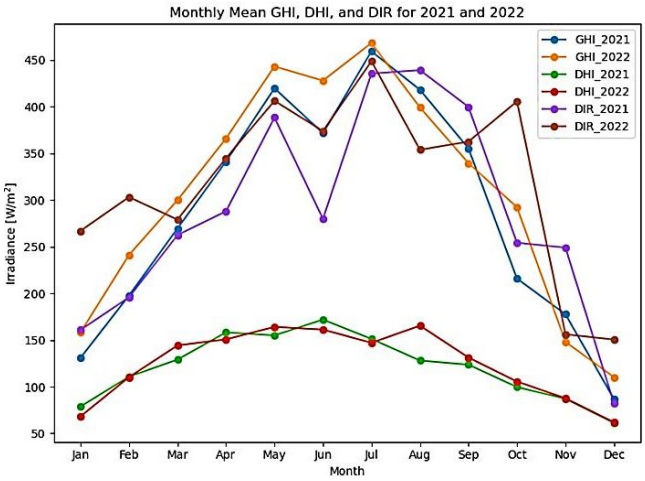

Fig. 2. Monthly mean values of GHI, DHI and DNI for 2021 and 2022 (color online)

Table 1. Average statistics of monthly mean GHI values

Month Year	Mean (W/m^2)	StDev	Median (W/m^2)	CV (%)	Min (W/m^2)	Max (W/m^2)	Q1 (W/m^2)	Q3 (W/m^2)
Jan 2021	130.88	68.15	142.28	52.06	19.81	221.25	72.595	203.25
Feb 2021	197.70	95.28	203.22	48.19	45.63	353.77	127.52	276.59
Mar 2021	269.52	127.00	288.89	47.12	42.71	455.00	182.97	374.93
Apr 2021	341.31	129.92	366.24	38.06	92.16	499.30	261.41	459.58
May 2021	419.72	121.93	453.50	29.05	93.02	576.44	379.52	506.11
Jun 2021	371.64	114.49	400.45	30.80	109.54	515.72	294.37	462.04
Jul 2021	459.35	53.67	469.36	11.68	305.12	525.78	431.85	498.20
Aug 2021	418.12	93.68	456.14	22.40	186.31	510.71	409.96	473.59
Sep 2021	355.35	92.03	392.57	25.89	107.83	447.69	303.63	417.98
Oct 2021	215.92	114.28	262.46	52.92	34.16	400.56	108.82	293.47
Nov 2021	177.56	70.96	183.85	39.96	23.86	285.72	133.54	238.14
Dec 2021	86.85	58.46	59.65	67.30	21.15	214.68	37.35	135.60
Jan 2022	158.08	74.69	193.46	47.24	23.07	253.42	98.12	220.71
Feb 2022	241.12	75.77	266.55	31.42	108.12	386.19	183.61	295.11
Mar 2022	299.88	110.10	311.92	36.71	77.05	456.12	207.12	387.31
Apr 2022	365.95	127.16	396.80	34.74	83.50	504.34	310.08	468.30
May 2022	443.18	88.19	466.94	19.89	207.73	539.13	406.16	513.03
Jun 2022	427.98	94.19	456.52	22.00	179.59	545.53	409.26	497.45
Jul 2022	468.24	72.08	486.43	15.39	216.21	543.04	459.03	511.23
Aug 2022	399.25	55.83	412.94	13.98	277.15	481.87	373.53	438.80
Sep 2022	339.60	91.48	356.87	26.94	70.38	465.82	316.87	401.40
Oct 2022	292.29	56.71	296.38	19.40	157.67	412.08	257.60	330.2
Nov 2022	148.09	81.74	125.55	55.19	31.54	273.46	76.67	244.26
Dec 2022	110.14	66.94	86.69	60.77	28.23	217.07	51.20	175.22

StDev – standard deviation; Q1 – first quartile; Q3 – third quartile; CV – coefficient of variation

Fig. 3 illustrates the monthly mean longwave downward radiation (LWRD) and temperature for 2021 and 2022, with the corresponding statistical details provided in Table 2. In 2021, the monthly mean LWRD reached its maximum in July at 382 W/m², while in 2022, the peak LWRD occurred in August, with a slightly higher value at 387 W/m². These peaks typically occur during the summer months, when increased surface temperatures and water vapor contribute to enhanced longwave radiation emission from the atmosphere [24].

The lowest monthly mean LWRD values were observed in January, with 2022 showing marginally lower levels (266 W/m²) compared to 2021 (283 W/m²). This seasonal minimum is expected during winter months when colder temperatures and lower humidity lead to a decrease in longwave radiation reaching the surface. The LWRD remained relatively stable from January to March in both years, followed by a pronounced increase starting in April, signalling the seasonal transition towards warmer conditions and increasing atmospheric moisture.

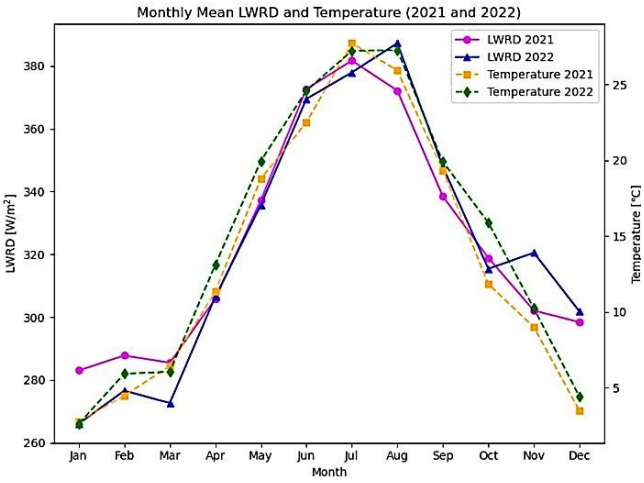

Fig. 3. Monthly mean LWRD and temperature for year 2021 and 2022 at BSRN INO station (color online)

Table 2. Average Statistics of monthly mean LWRD values

Month Year	Mean (W/m^2)	StDev	Median (W/m^2)	CV (%)	Min (W/m^2)	Max (W/m^2)	Q1 (W/m^2)	Q3 (W/m^2)
Jan 2021	283.01	34.00	290.83	12.01	210.03	343.59	260.44	309.48
Feb 2021	287.79	31.01	288.53	10.77	205.85	333.71	272.94	313.51
Mar 2021	285.45	26.09	284.13	9.14	238.92	335.53	265.73	303.71
Apr 2021	305.84	31.15	307.69	10.18	253.61	351.41	281.23	337.17
May 2021	337.26	24.39	340.44	7.23	281.20	375.07	321.47	354.28
Jun 2021	372.62	19.14	373.14	5.13	344.97	410.88	355.68	385.59
Jul 2021	381.70	13.75	383.51	3.60	354.26	404.32	371.90	389.29
Aug 2021	372.16	18.64	373.64	5.00	327.60	398.76	359.66	387.52
Sep 2021	338.46	18.27	334.96	5.39	310.23	385.98	325.08	354.18
Oct 2021	318.87	30.02	322.67	9.41	261.97	361.77	291.51	345.30
Nov 2021	302.10	26.59	308.54	8.80	248.80	337.55	285.09	321.94
Dec 2021	298.40	31.32	309.66	10.49	222.25	336.99	288.73	320.34
Jan 2022	266.05	34.27	257.31	12.88	214.13	333.08	241.44	291.29
Feb 2022	276.57	22.80	273.06	8.24	235.36	326.83	262.68	290.66
Mar 2022	272.64	27.17	270.58	9.96	229.71	353.21	258.69	285.58
Apr 2022	306.52	25.95	309.40	8.46	257.15	360.16	291.32	326.05
May 2022	335.64	26.18	340.58	7.80	294.69	376.93	311.77	354.94
Jun 2022	369.48	13.68	368.41	3.70	331.00	391.07	361.93	380.64
Jul 2022	377.93	17.50	382.80	4.63	344.66	402.55	364.92	392.74
Aug 2022	387.26	9.41	388.30	2.43	365.37	402.20	381.03	394.71
Sep 2022	347.94	28.56	348.34	8.20	291.77	393.26	325.96	373.24
Oct 2022	315.38	21.41	318.63	6.79	277.85	369.55	302.32	328.25
Nov 2022	320.52	18.91	320.33	5.90	281.18	364.26	310.66	333.47
Dec 2022	301.83	28.13	302.31	9.32	232.00	337.94	282.43	327.42

StDev – standard deviation; Q1 – first quartile; Q3 – third quartile; CV – coefficient of variation

3.2. Diurnal variation of global radiation

The hourly averages of GHI values are shown in Fig. 4. In order to remove potential artefacts in the dataset, we used the measured data with solar zenith angle below 85 degrees. As expected, the highest GHI values were recorded around solar noon. In July 2021, the peak GHI reached 829 W/m^2, while in 2022, it increased slightly to 842 W/m^2, indicating a reduction in cloudiness. In December, the highest GHI values were 164 W/m^2, in 2021, and 202 W/m^2, in 2022. Similar values were reported by Blaga and Paulescu [25] for the Western region of Romania. The monthly trends for both years were generally consistent, except for February and

October, where the GHI values were slightly higher in 2022 compared to 2021. The time, when the highest GHI value is recorded in 2021, shifts with one hour from late autumn and spring to late spring, summer and early autumn (Fig. 4a). However, in 2022, in most of the months, the highest GHI values were recorded at 12 pm (local time), while only in July and April, the GHI values were highest at 1 pm, and in August at 11 am (Fig. 4b). These variations highlight the influence of seasonal and atmospheric changes on the timing of maximum solar irradiance throughout the year.

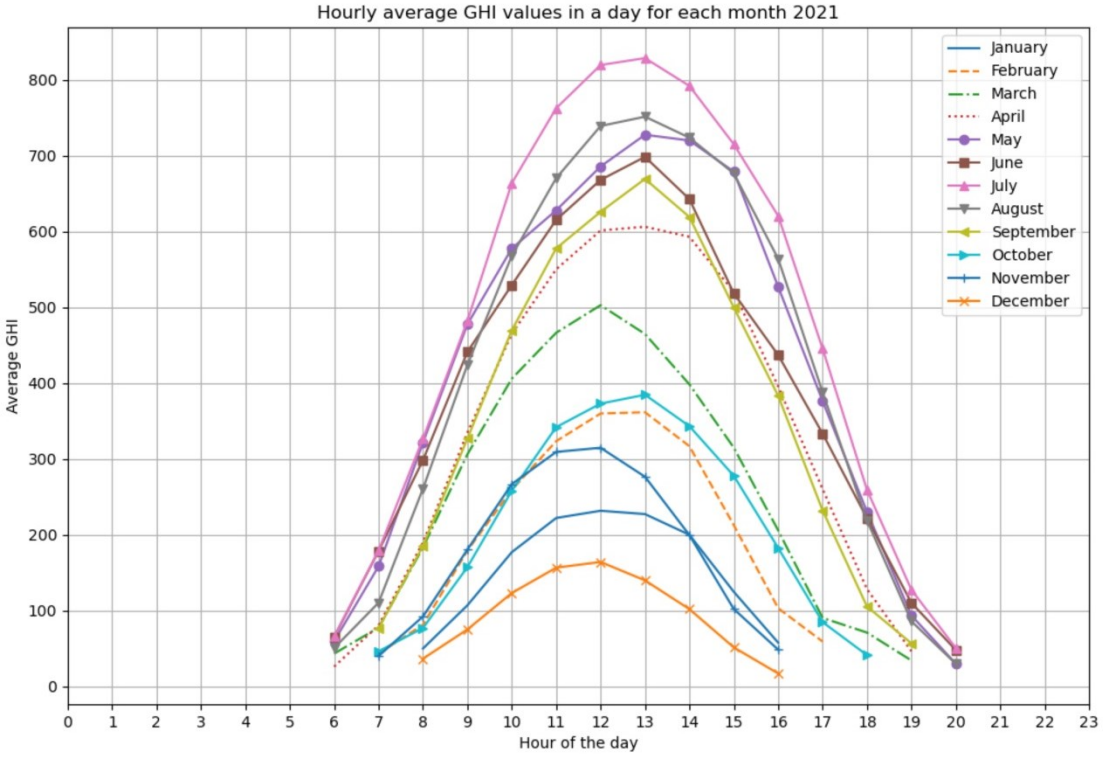

(a)

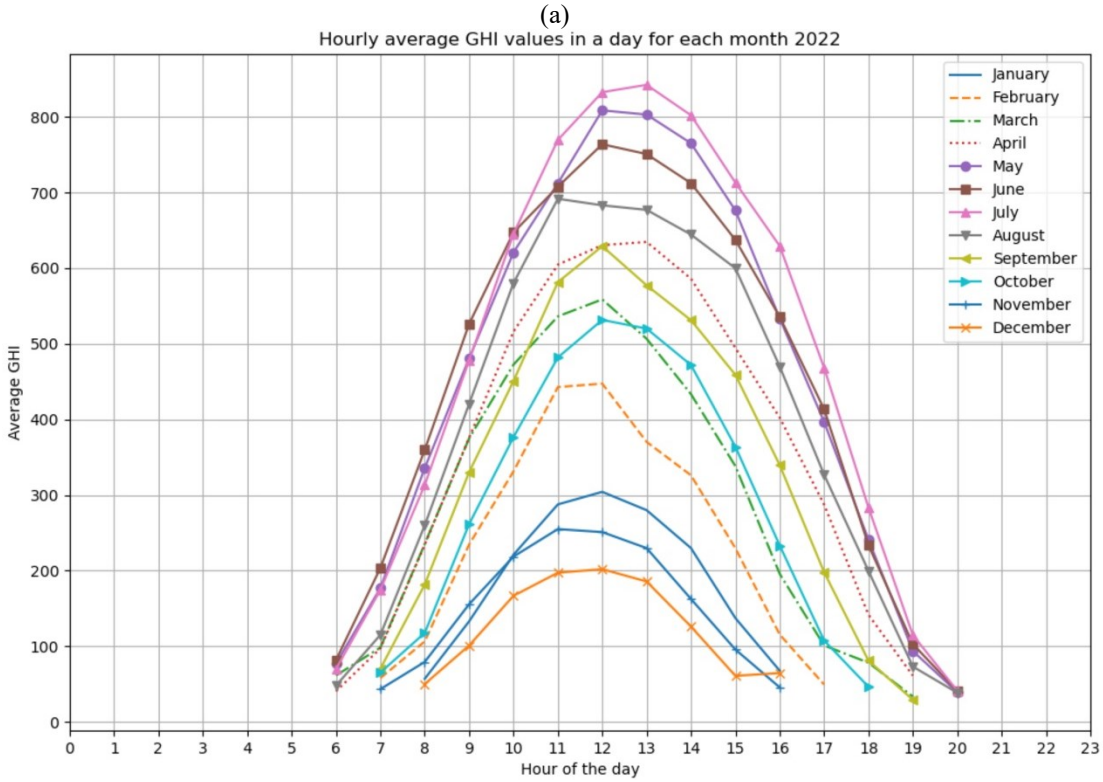

(b)

Fig. 4. Daily evolution of the monthly mean hourly global irradiance (Wm^{-2}) at BSRN INO, local time: (a) 2021, (b) 2022 (color online)

The accumulated GHI indicates the total energy received by the ground surface over a specific period [9]. Fig. 5 presents the monthly accumulated GHI for 2021 and 2022. In both years, substantially higher accumulated GHI was obtained in July (maximum of 7,136.44 W/m^2 in 2021 and 7,177.90 W/m^2 in 2022), compared to the rest of the months. This pattern is driven by the longer daylight hours and higher solar elevation during the peak of summer, along with reduced cloud cover (as shown in Fig. 6). However, variations were observed between the two years for other months. For example, in 2021, May and August displayed similar accumulated GHI values, while in 2022, May and June had comparable values. Additionally, in 2021, April and September had nearly identical accumulated GHI, while the following year, higher values were obtained in April compared to September. In both years, the lowest accumulated GHI was observed in December (862.79 W/m^2 in 2021 and 1,153.56 W/m^2 in 2022). This is consistent with the reduced solar input during winter and the increased cloudiness during this month (Fig. 6).

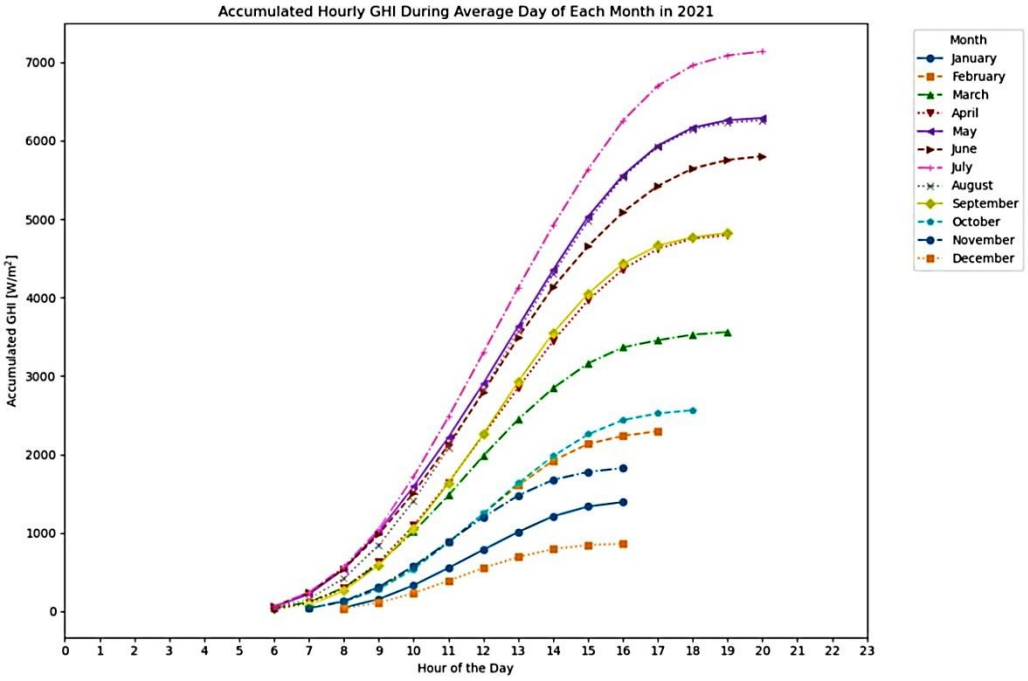

(a)

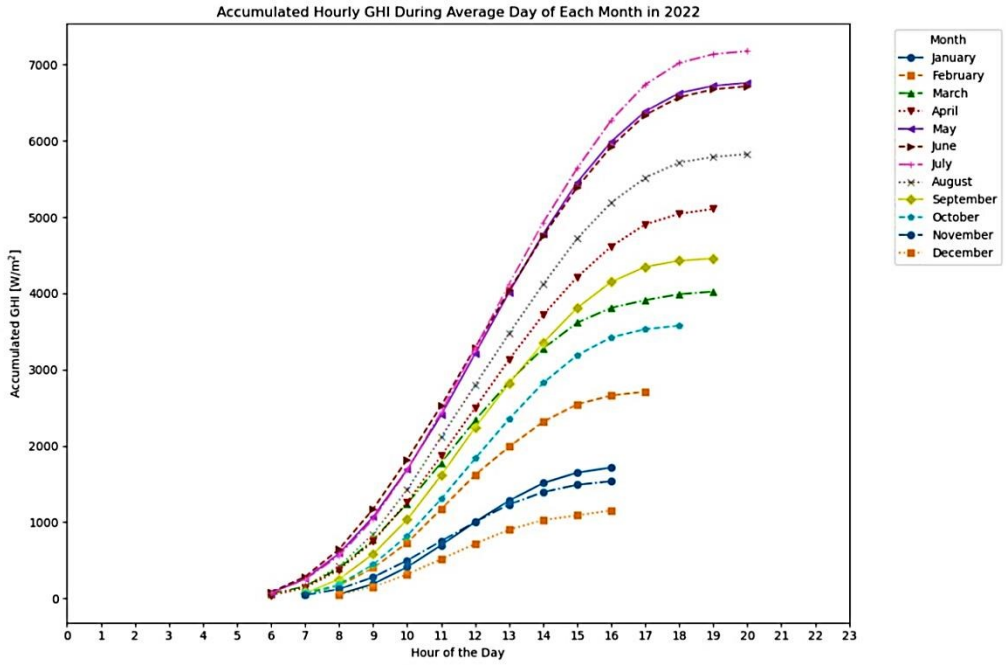

(b)

Fig. 5. Accumulated hourly global solar irradiation during an average day of each month at BSRN INO local time: (a) 2021, (b) 2022 (color online)

3.3. Clearness index

The daily clearness index indicates the clearness of the atmosphere and is defined as the ratio of the global radiation to the extraterrestrial radiation ($K_T = G_d/G_{0d}$) [9]. K_T values below 0.35 indicate extreme cloudy periods, K_T values between 0.35 and 0.65 indicate partly cloudy days, while values above 0.65 represent clear skies [26]. According to Kalogirou et al. [9], locations with high clear day frequencies are most suited to solar energy conversion systems with concentrating devices and locations with partly cloudy days are more suited to systems with non-concentrating devices.

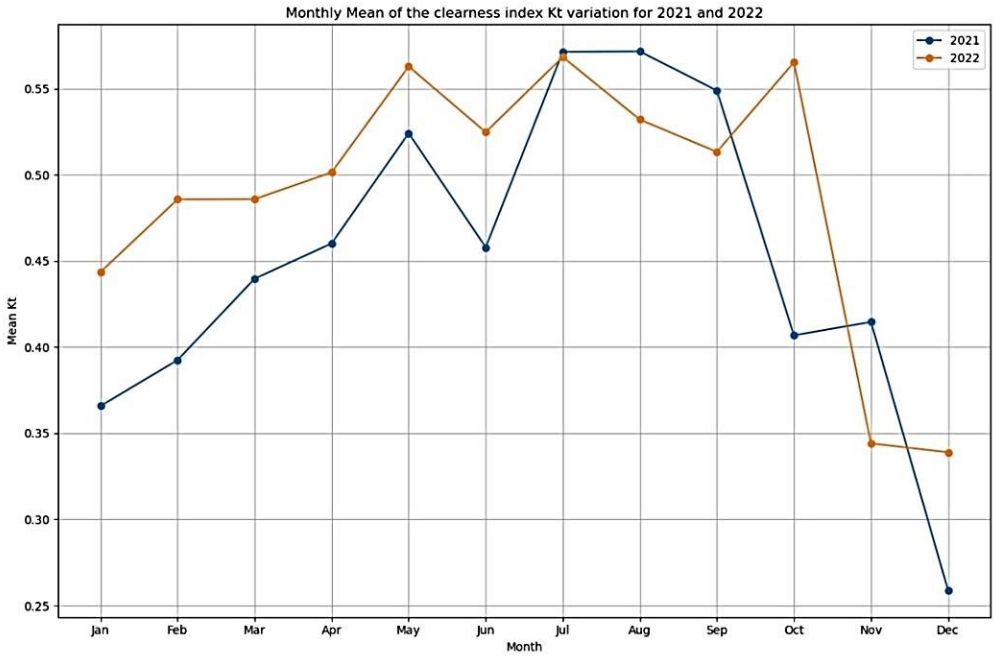

Fig. 6. Monthly variation of the clearness index (K_T) at BSRN INO (color online)

Table 3. Statistics of monthly mean clearness index for 2021

Month Year	Mean	StDev	Median	CV (%)	Min	Max	Q1	Q3
Jan 2021	0.36	0.18	0.36	51.48	0.05	0.66	0.19	0.54
Feb 2021	0.39	0.17	0.40	43.90	0.10	0.61	0.26	0.55
Mar 2021	0.43	0.20	0.48	46.82	0.07	0.70	0.29	0.61
Apr 2021	0.46	0.19	0.49	42.02	0.10	0.71	0.31	0.64
May 2021	0.52	0.15	0.52	29.94	0.10	0.72	0.46	0.64
Jun 2021	0.45	0.15	0.49	33.44	0.10	0.64	0.32	0.55
Jul 2021	0.57	0.06	0.58	11.89	0.39	0.65	0.54	0.62
Aug 2021	0.57	0.10	0.60	18.87	0.26	0.68	0.54	0.64
Sep 2021	0.54	0.13	0.61	24.71	0.21	0.68	0.51	0.64
Oct 2021	0.40	0.22	0.46	55.02	0.06	0.66	0.19	0.62
Nov 2021	0.41	0.17	0.45	43.25	0.05	0.65	0.28	0.56
Dec 2021	0.25	0.16	0.18	65.98	0.06	0.64	0.12	0.42
Jan 2022	0.44	0.20	0.48	45.19	0.07	0.66	0.29	0.62
Feb 2022	0.48	0.15	0.53	31.99	0.20	0.69	0.33	0.57
Mar 2022	0.48	0.15	0.51	31.37	0.13	0.70	0.38	0.61
Apr 2022	0.50	0.18	0.55	36.03	0.11	0.71	0.43	0.64
May 2022	0.56	0.11	0.60	21.25	0.28	0.70	0.49	0.64
Jun 2022	0.52	0.12	0.56	23.77	0.19	0.70	0.45	0.61
Jul 2022	0.56	0.09	0.58	17.37	0.25	0.68	0.54	0.63
Aug 2022	0.53	0.08	0.56	16.15	0.29	0.64	0.49	0.59
Sep 2022	0.51	0.15	0.55	29.90	0.10	0.68	0.46	0.63
Oct 2022	0.56	0.11	0.59	19.82	0.28	0.69	0.52	0.65
Nov 2022	0.34	0.17	0.30	51.66	0.07	0.63	0.22	0.52
Dec 2022	0.33	0.20	0.26	60.71	0.08	0.67	0.16	0.55

StDev – standard deviation; Q1 – first quartile; Q3 – third quartile; CV – coefficient of variation

At INO station, the annual average K_T value was 0.45 in 2021 and 0.48 in 2022. From the beginning of the year towards late Autumn, monthly mean K_T values were above 0.35 (Fig. 6). The highest K_T value occurred in July and August, 0.57 for 2021, while the lowest occurred in December, 0.25 for 2021 (Table 3).

In 2021, in January, May and December, the median values were lower or equal to the average values, while in 2022, lower median values were obtained only in November and December. However, only in August and September 2021, and in May 2022 the median value exceeded 0.60.

The CV values indicated that the most stable conditions were observed in July, August and September 2021 (12% – 25%), and the least stable in December 2021 (66%), while for 2022, the most stable conditions were observed in May, June, July, August and October (16% – 24%), and the least stable in December (61%). The results indicated that non-concentrating solar conversion systems are suited to the INO station region for most of the year, when there is a high frequency of partly cloudy days, and solar energy conversion systems with concentrating devices during the summer period [9].

4. Conclusions

This study presented an overview of the irradiation data statistical analysis over a two-year period of INO station operation (2021-2022). The irradiance levels at Bucharest are representative of the latitude belt of 45°N. However, discrepancies can be observed when compared to other locations at the same latitude, primarily attributed to variations in cloud cover and altitude. For example, according to the Global Solar Atlas platform [27], which utilizes data from SOLARGIS [28], the annual Global Horizontal Irradiation (GHI) at Bucharest (44.43°N, 26.11°E, 75 m a.s.l.) is 1,378.9 kWh/m². In contrast, Aosta (45.73°N, 7.32°E, 585 m a.s.l.) records a higher GHI of 1,454.6 kWh/m², attributed to its higher altitude and reduced cloud cover. Conversely, Toronto (43.65°N, 79.38°W) exhibits almost identical GHI levels to Bucharest, at 1,382.9 kWh/m², suggesting comparable yearly cloud coverage.

The analysis of GHI and its components, DNI and DHI, over 2021 and 2022, highlighted key fluctuations in GHI. A larger variation was seen in 2021, compared to 2022, and significant DNI contribution, especially in July for both years. Statistical evaluation revealed that median GHI values were typically below mean values, suggesting data skewness, except in peak sunshine months. The coefficient of variation confirmed higher instability in solar radiation compared to the Mediterranean region, being relatively stable only during summer.

LWRD trends peaked in summer and decreased in the cooler months, with a slight dip in 2022 compared to 2021. Diurnal GHI patterns consistently showed high solar radiation levels around noon, with small shifts in the timing of peak radiation between the two years.

The highest accumulated GHI values in both years were recorded in July, month that emerged as pivotal for solar energy harvesting. The clearness index predominantly signalled conditions favouring non-concentrating solar conversion systems, with summer months being conducive for solar energy conversion systems with concentrating devices, due to the high frequency of clear days. These findings emphasize the need to implement adaptive solar energy solutions, attuned to seasonal and meteorological patterns, in order to optimize sustainable energy capture throughout varying environmental conditions.

Data availability

The data can be accessed from the PANGEA website: https://www.pangaea.de/?q=BSRN&f.author%5B%5D=Carstea%2C+Emil.

Acknowledgements

The author E.C. acknowledges the support of the Romanian Ministry of Research, Innovation and Digitalization through the Core Program within the National Research Development and Innovation Plan 2022-2027, Project PN 23 05.

References

[1] D. L. Hartmann, A. M. G. Klein Tank, M. Rusticucci, L. V. Alexander, S. Brönnimann, Y. Charabi, F. J. Dentener, E. J. Dlugokencky, D. R. Easterling, A. Kaplan, B. J. Soden, P. W. Thorne, M. Wild, P. M. Zhai, "Climate Change 2013: The Physical Science Basis. Contribution of Working Group I to the Fifth Assessment Report of the Intergovernmental Panel on Climate Change", Cambridge University Press, Cambridge, United Kingdom, 159 (2013).

[2] L. H. Luo, L. G. Wang, Y. L. Liang, L. Zhang, Y. J. Wang, Optoelectron. Adv. Mat. **16**(7-8), 373 (2022).

[3] H. A. Mohamed, E. K. Shokr, M. M. Wakkad, N. M. A. Hadia, Y. A. Taya, Optoelectron. Adv. Mat. **16**(5-6), 209 (2022).

[4] L. G. Wang, L. Z. Wang, Z. H. Liu, Y. F. Li, L. Zhang, Optoelectron. Adv. Mat. **18**(1-2), 32 (2024).

[5] P. Kwaśnicki, Clean. Eng. Technol. **22**, 100810 (2024).

[6] L. V. Assiene Mouodo, A. H. M. Ali, S. M. Olivier Thierry, A. D. Moteyo, J. Gaston Tamba, P. Axaopoulos, Helyon **10**, e36670 (2024).

[7] M. Louazni, A. Khouya, A. Al-Dahidi, M. Mussetta, K. Amechnoue, Optik **199**, 163379 (2019).

[8] H. Braun, S. T. Buddha, V. Krishnan, C. Tepedelenlioglu, A. Spanias, M. Banavar,

D. Srinivasan, Sustain. Energy, Grids Netw. **6**, 58 (2016).
[9] S. A. Kalogirou, S. Pashiardis, A. Pashiardi, Renew. Energy **101**, 1102 (2017).
[10] B. Durusoy, T. Ozden, B. G. Akinoglu, Sci. Rep. **10**, 13300 (2020).
[11] C. P. Castillo, F. B. e Silva, C. Lavalle, Energ. Policy **88**, 86 (2016).
[12] R. Pravalie, I. Sirodoev, J. Ruiz-Arias, M. Dumitrascu, Renew. Energy **193**, 976 (2022).
[13] https://data.gov.ro/dataset/harta-potentialului-energetic-solar
[14] U. Pfeifroth, S. Kothe, J. Drücke, J. Trentmann, M. Schröder, N. Selbach, R. Hollmann, Surface Radiation Data Set - Heliosat (SARAH) - Edition 3, Satellite Application Facility on Climate Monitoring, (2023) DOI:10.5676/EUM_SAF_CM/SARAH/V003, https://doi.org/10.5676/EUM_SAF_CM/SARAH/V003.
[15] A. Ohmura, H. Gilgen, H. Hegner, G. Müller, H. Lüthy, E. G. Dutton, Bull. Am. Meteorol. Soc. **79**(10), 2115 (1998).
[16] M. Wild, D. Folini, C. Schär, N. Loeb, E. G Dutton, G. König-Langlo, PANGAEA, (2013).
[17] V. Nicolae, L. Belegante, J. Vasilescu, A. Nemuc, F. Toanca, O. G. Tudose, C. Radu, D. Nicolae, J. Optoelectron. Adv. M. **25**(3-4), 176 (2023).
[18] https://environment.inoe.ro/category/31/business-card
[19] I. Reda, A. Andreas, NREL Report No. TP-560-34302, 55 (2003).
[20] W. Holmgren, C. Hansen, M. Mikofski, J. Open Source Softw. **3**(29), 884 (2018).
[21] K. Fragkos, B. Antonescu, D. M. Giles, D. Ene, M. Boldeanu, G. A. Efstathiou, L. Belegante, D. Nicolae, Atmos. Meas. Tech. **12**, 1979 (2019).
[22] C. N. Long, E. G. Dutton, BSRN Global Network recommended QC tests, V2.x, (2002).
[23] C. N. Long, Y. Shi, Open Atmos. Sci. J. **2**, 23 (2008).
[24] S. Pashiardis, S. A. Kalogirou, Appl. Sci. **11**(2), 719 (2021).
[25] R. Blaga, M. Paulescu, Sol. Energy **174**, 608 (2018).
[26] A. Kudish, A. Ianetz, Energy Convers. Manag. **37**(4), 405 (1996).
[27] https://globalsolaratlas.info/map
[28] T. Cebecauer, M. Suri, Energy Procedia **69**, 1958 (2015).

*Corresponding author: emil.carstea@inoe.ro